Figure S1

A

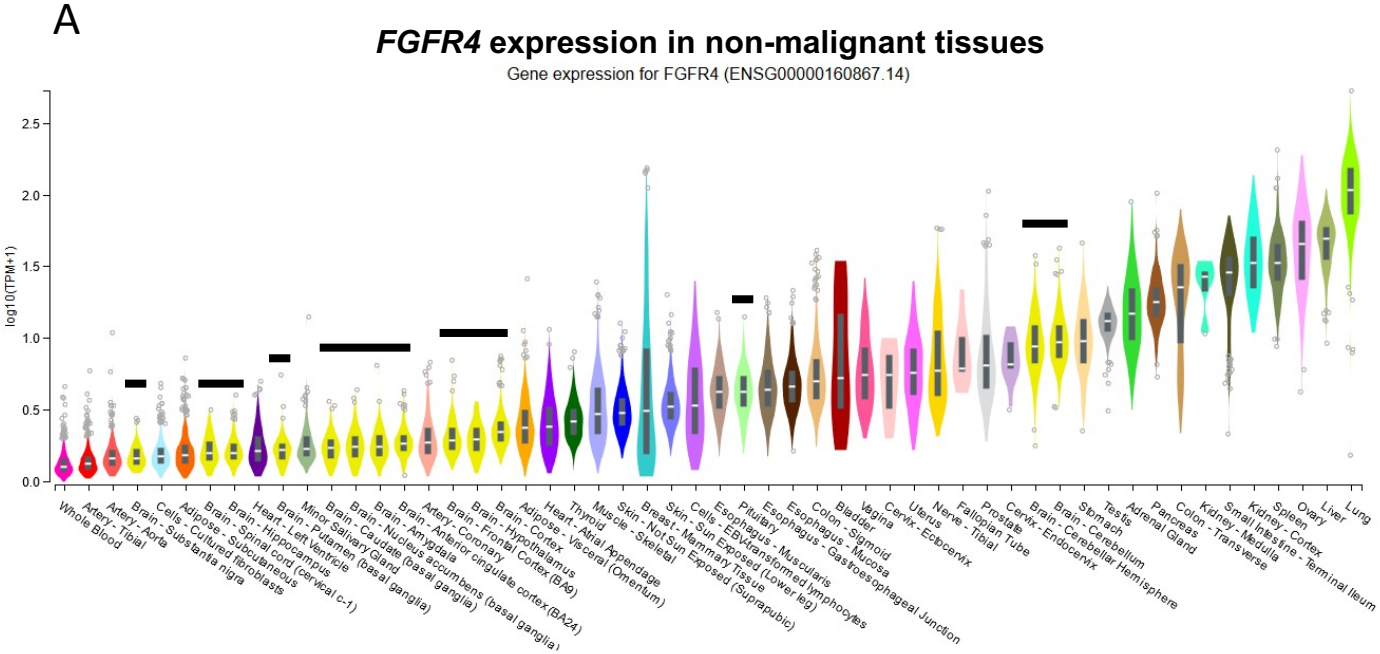

B

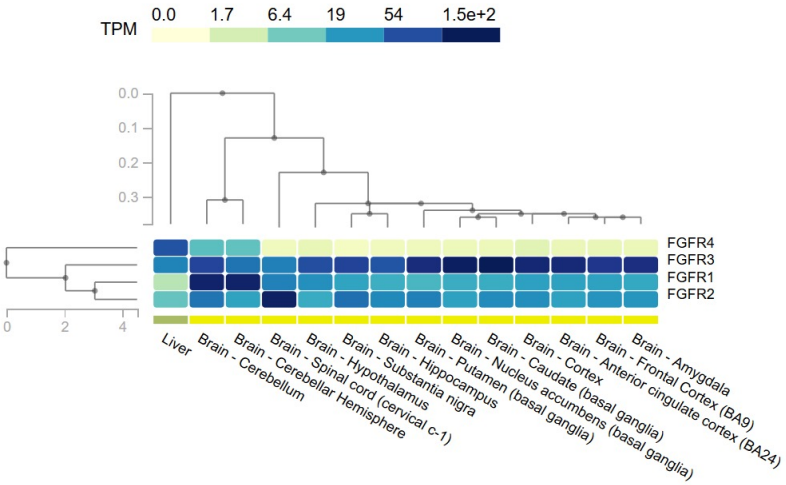

C

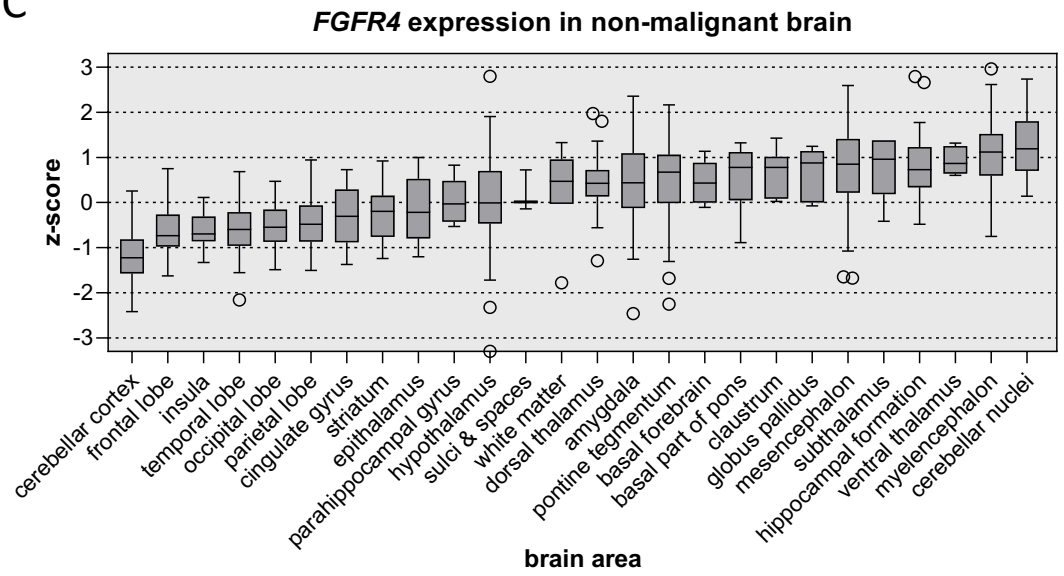

Supplementary Figure S1. *FGFR4* expression is comparably low in the brain and differs in between brain regions. (A) *FGFR4* mRNA expression levels were compared between non-malignant human organs, including different brain regions (indicated by black bars). RNA sequencing data from the Genotype-Tissue Expression (GTEx) Project data set were used. Data are given as log10 transformed transcript per million (TPM) reads. **(B)** Expression levels of the FGFR family members in different brain regions and the liver are shown. Data were obtained from the GTEx project given as TPM. **(C)** *FGFR4* mRNA expression is shown in different adult non-malignant brain areas. Data were obtained from the *Allen brain atlas (brain-map.org)* and are presented as z-scores (box-whiskers: Tukey).

Figure S2

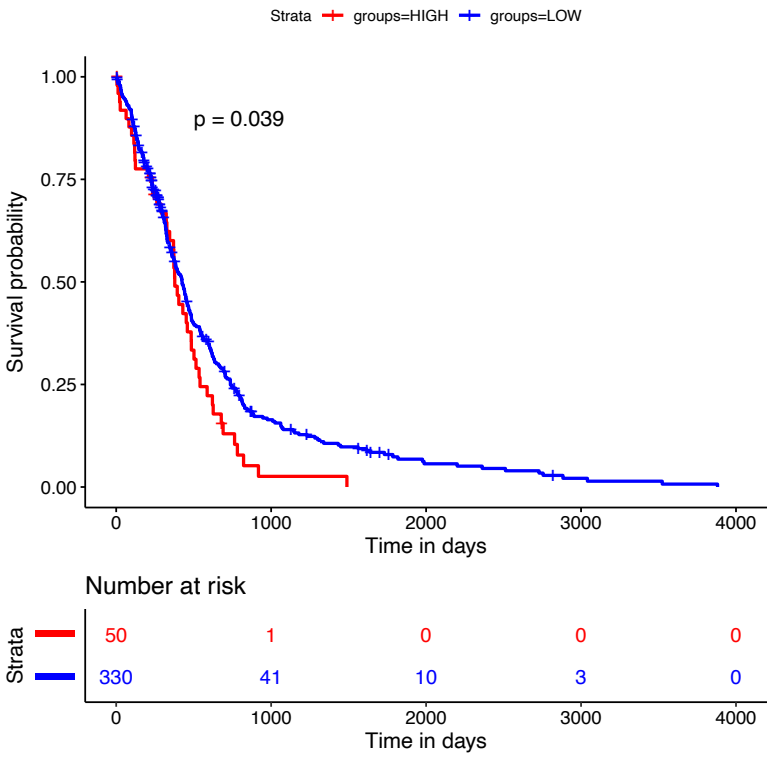

Supplementary Figure S2. *FGFR4* expression is associated with worse prognosis in GBM patients. Survival of patients with high (red, n=50) or low (blue, n=330) *FGFR4*-expressing GBM from the TCGA-GBM-395.MAS5.0-u133a data set is shown. Cutpoints for *FGFR4* stratification were determined by maximally selected rank statistics. Statistical analyses: Log-rank tests

Figure S3

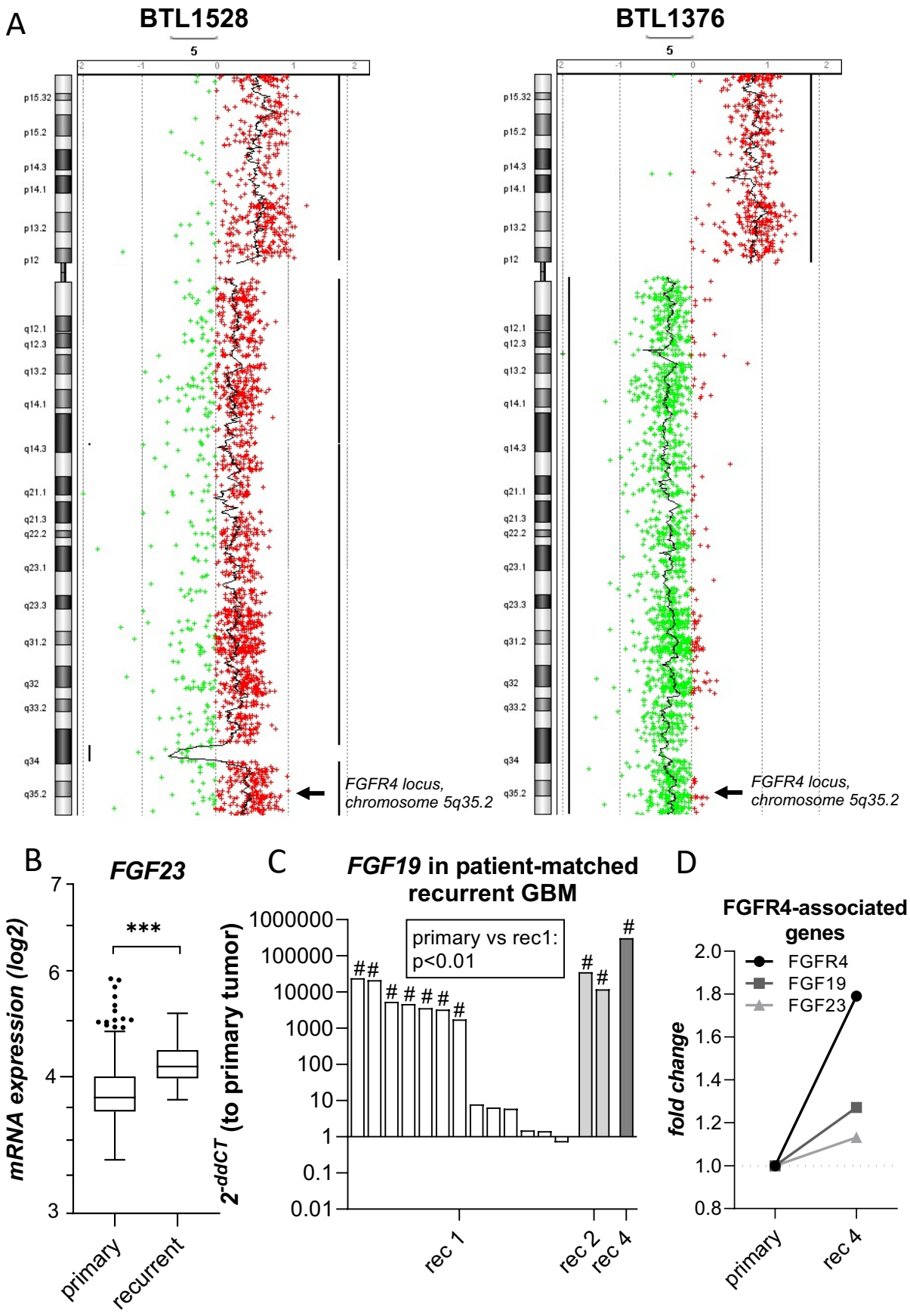
A
BTL1528
BTL1376
FGFR4 locus, chromosome 5q35.2
FGFR4 locus, chromosome 5q35.2
B
FGF23
mRNA expression (log2)
***
primary
recurrent
C
FGF19 in patient-matched recurrent GBM
2-ddCT (to primary tumor)
primary vs rec1: p<0.01
rec 1
rec 2
rec 4
D
FGFR4-associated genes
FGFR4
FGF19
FGF23
fold change
primary
rec 4

Supplementary Figure S3. *FGFR4*^{high} GBM models lack *FGFR4* gene dose alterations, but *FGFR4* ligand genes are overexpressed in recurrent GBM. (A) Chromosome 5 profiles from array comparative genomic hybridization of *FGFR4*^{high} GBM cells BTL1528 and BTL1376 are shown. The gene dose (log2 ratio of tumor DNA/non-malignant DNA) is depicted. The arrow indicates the chromosomal locus of *FGFR4*. red = gains, green = losses. **(B)** *FGF23* mRNA expression in primary (n=497) and recurrent GBM (n=16) was analyzed in the TCGA-GBM-HG-U133A data set. Statistical significance was analyzed by Student's t-test. *** p<0.001 **(C)** *FGF19* mRNA levels were determined by qRT-PCR patient-matched primary GBM (n=14) and sequential recurrences (rec1, n=13; rec2, n=2; rec4, n=1). Statistical analyses: Student's t-test. # indicate recurrent lesions matching to primary tumors with undetectable *FGF19* expression after 50 cycles (CT >50), thus, arbitrarily set to 50 for normalization approaches. **(D)** mRNA expression levels of *FGFR4* and associated ligand genes *FGF19* and *FGF23* derived from whole genome gene expression arrays are shown in primary tumor (set to 1) and the 4th recurrence of one GBM patient.

Figure S4

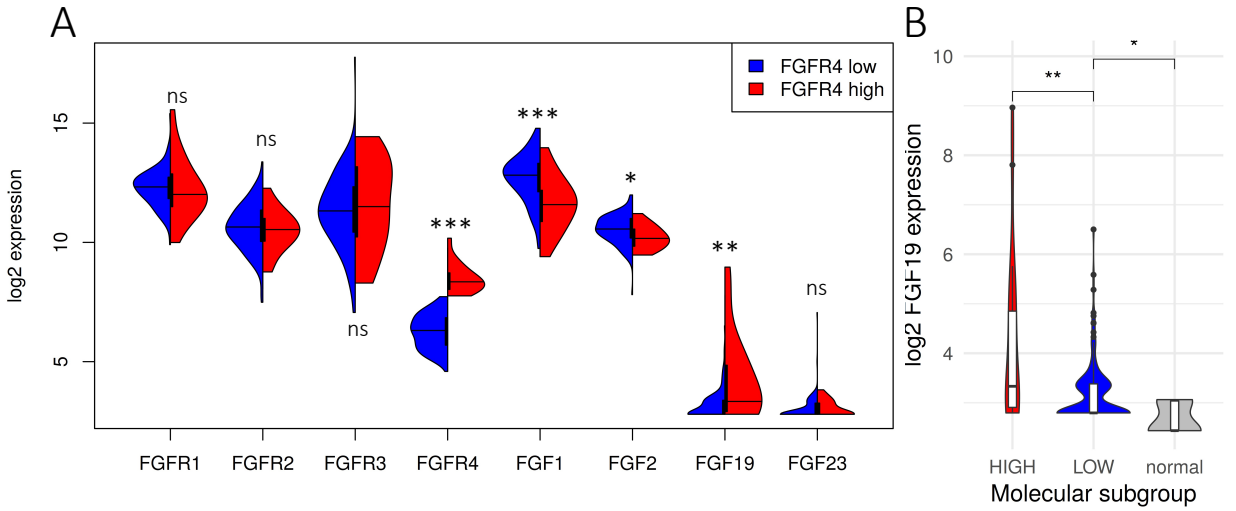
A
log2 expression
FGFR4 low
FGFR4 high
ns
ns
ns
***
***
*
**
ns
FGFR1
FGFR2
FGFR3
FGFR4
FGF1
FGF2
FGF19
FGF23
B
log2 FGF19 expression
**
*
HIGH
LOW
normal
Molecular subgroup

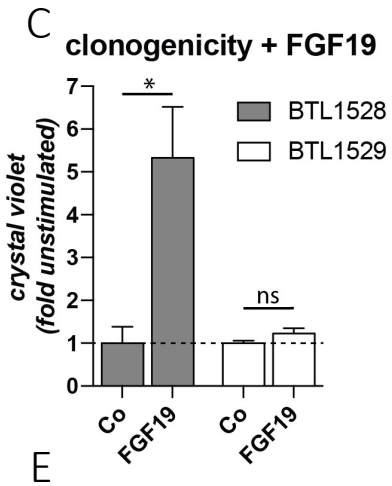
C
clonogenicity + FGF19
crystal violet (fold unstimulated)
BTL1528
BTL1529
*
ns
Co
FGF19
Co
FGF19

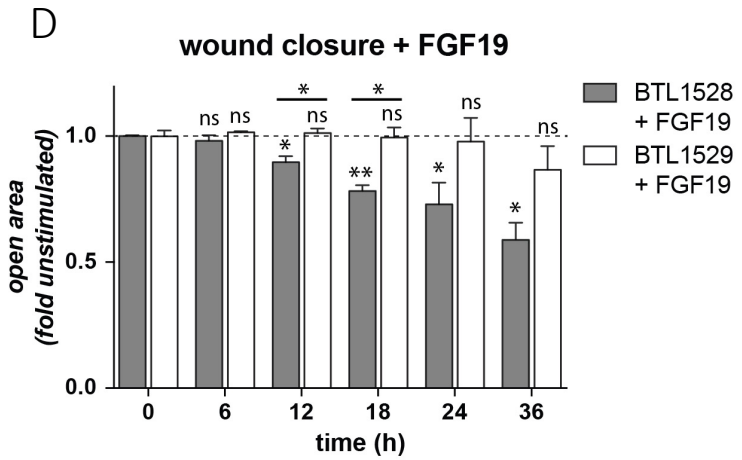
D
wound closure + FGF19
open area (fold unstimulated)
BTL1528 + FGF19
BTL1529 + FGF19
time (h)

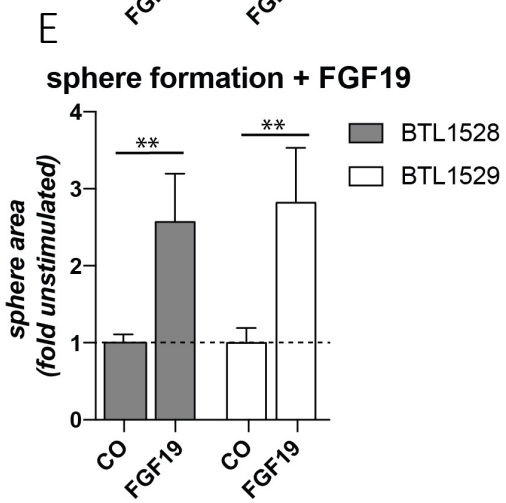
E
sphere formation + FGF19
sphere area (fold unstimulated)
BTL1528
BTL1529
**
**
CO
FGF19
CO
FGF19

Supplementary Figure S4. FGF19 promotes hallmarks of GBM aggressiveness. (A+B) TCGA-GBM RNA sequencing data were analyzed and stratified into *FGFR4*^{high} (red) and *FGFR4*^{low} (blue) subgroups. **(A)** mRNA expression levels of the indicated FGF/FGFR family members in the *FGFR4*^{high} (red) and *FGFR4*^{low} (blue) GBM subgroups are depicted as violin plots (median ± SD). **(B)** *FGF19* expression levels are depicted in the indicated GBM subgroups and in non-malignant brain (grey). **(C)** Clonogenicity, **(D)** wound-healing assays, **(E)** and sphere formation assays upon stimulation with FGF19 are shown. Endogenously *FGFR4*^{high} BTL1528 and *FGFR4*^{low} BTL1529 GBM cells were seeded in serum-supplemented growth medium. After 24h, serum was deprived in **(C)** and cells were stimulated with FGF19-conditioned medium (50ng/ml) in **(C-E,** mean +/- SEM**)**. Effects were observed after 7 days **(C)**, over time as indicated **(D)**, or after 4 days **(E)**. Statistics: **(A+B)** Wilcoxon signed-rank test; **(C)** Student's t-tests; **(D+E)** 2-way ANOVA; * $p<0.05$, ** $p<0.01$, *** $p<0.001$, ns = not significant;

Figure S5

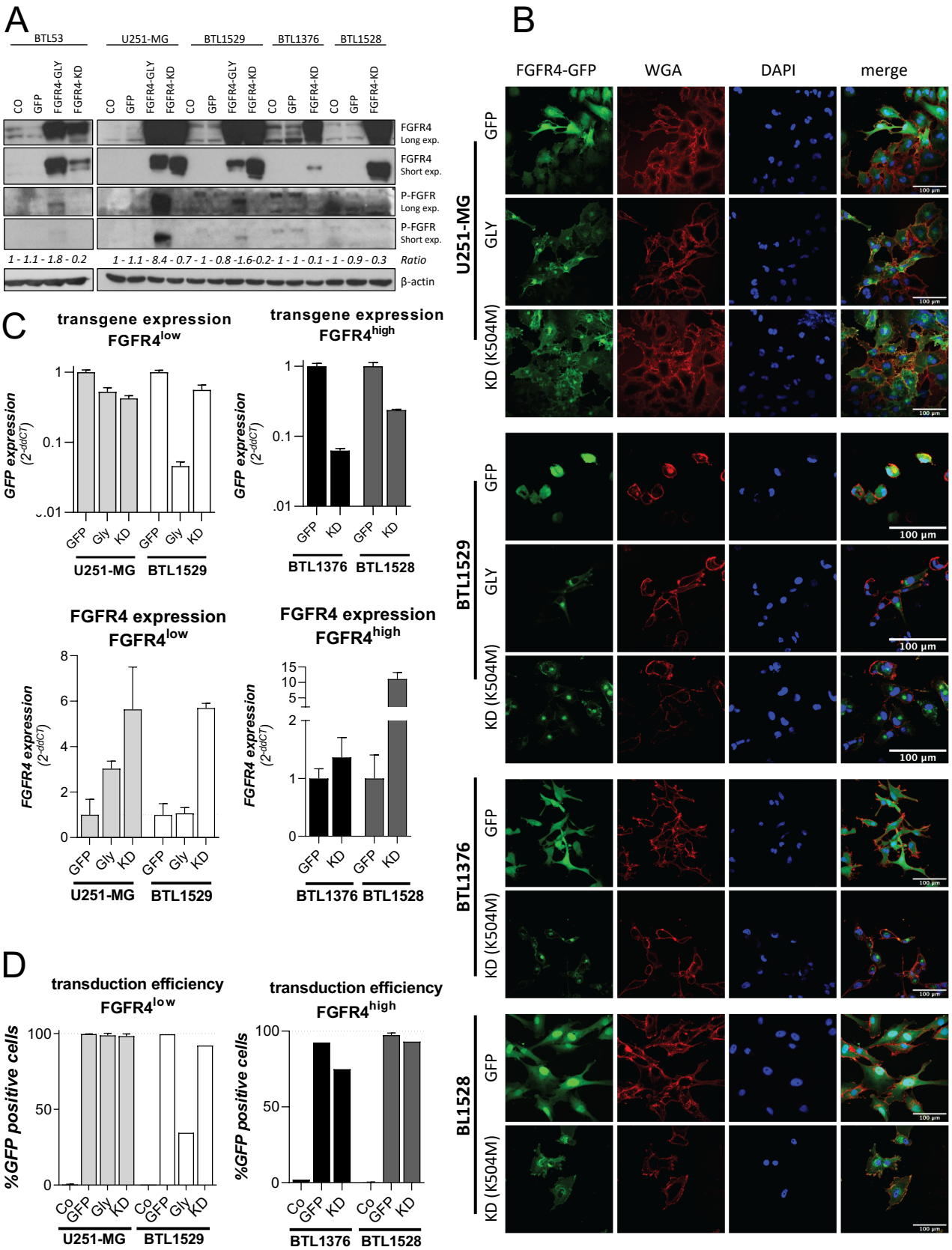
A
BTL53
U251-MG
BTL1529
BTL1376
BTL1528
CO
GFP
FGFR4-GLY
FGFR4-KD
FGFR4 Long exp.
FGFR4 Short exp.
P-FGFR Long exp.
P-FGFR Short exp.
1 - 1.1 - 1.8 - 0.2
1 - 1.1 - 8.4 - 0.7 - 1 - 0.8 -1.6-0.2- 1 - 1 - 0.1 - 1 - 0.9 - 0.3
Ratio
β-actin
B
FGFR4-GFP
WGA
DAPI
merge
U251-MG
BTL1529
BTL1376
BL1528
GFP
GLY
KD (K504M)
100 µm
C
transgene expression
FGFR4low
transgene expression
FGFR4high
GFP expression (2-ddCT)
GFP
Gly
KD
U251-MG
BTL1529
BTL1376
BTL1528
FGFR4 expression
FGFR4low
FGFR4 expression
FGFR4high
FGFR4 expression (2-ddCT)
D
transduction efficiency
FGFR4low
transduction efficiency
FGFR4high
%GFP positive cells
Co
GFP
Gly
KD

Supplementary Figure S5. Wild-type and kinase-dead FGFR4 transduction results in stably overexpressing GBM cell models. BTL1528 and BTL1376 (*FGFR4^{high}*) as well as BTL53, U251-MG, and BTL1529 (*FGFR4^{low}*) cells were transduced with retroviral constructs resulting in stable sublines overexpressing *GFP, FGFR4-Gly-GFP* or *FGFR4-KD(K504M)-GFP*. **(A)** FGFR4 expression and phosphorylation of FGFR proteins of the respective FGFR4-variant subclones and GFP-only-transduced cells (GFP) as compared to untransduced controls (Co) were analyzed by Western blotting of total protein lysates. β-actin served as loading control. Blots were normalized to the respective β-actin signal, and subsequently the ratios were calculated to show pathway activity in every cell model. **(B)** Confocal photomicrographs of the modified *FGFR4-GFP* or *GFP*-only cells as indicated counterstained with wheat germ agglutinin (WGA) and DAPI for plasma membrane and nuclear stain, respectively, are shown. Scale bars indicate 100µm. **(C)** *GFP (upper panel)* and *FGFR4 (lower panel)* mRNA expression levels are shown indicating the modified *FGFR4-GFP* transgenes in endogenously *FGFR4^{low} (left panel)* and *FGFR4^{high}* cells *(right panel).* Data are given as mean +/- SEM from three independent experiments normalized to *GFP*-only cells, set to 1 (2^{-ddCT}). **(D)** Transduction efficiency upon *FGFR4-Gly-GFP*, *FGFR4-KD (K504M)-GFP* or *GFP*-only overexpression was analyzed by flow cytometry testing for GFP-positive cells in endogenously *FGFR4^{low} (left panel)* and *FGFR4^{high} (right panel)* GBM models. Data are given as mean +/- SD from two independent experiments. GLY= *FGFR4-388Gly-GFP*, KD = *FGFR4 kinase-dead (K504M)-GFP*

Figure S6

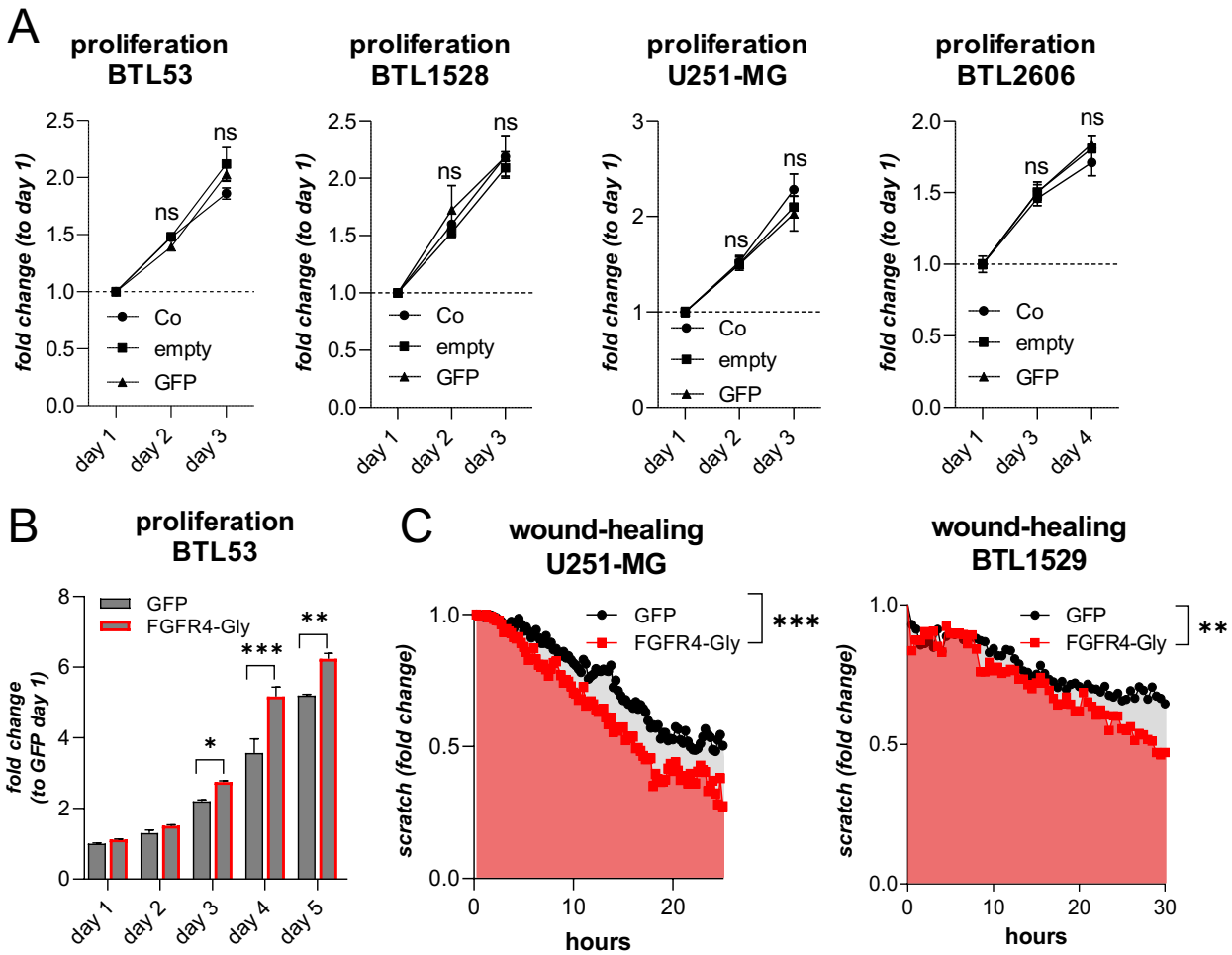

Supplementary Figure S6. ***FGFR4*** **overexpression promotes proliferation and wound healing capacity of endogenously** ***FGFR4^{low}*** **GBM cells. (A)** Proliferation capacity of control cells, as compared to stable empty-vector- and GFP-transduced GBM subclones. ns=not significant. **(B)** Proliferation capacity of *FGFR4-Gly*-overexpressing BTL53 GBM cells versus *GFP*-transduced sublines is shown. Two-way ANOVA: *p<0.05, **p<0.01, ***p<0.001 **(C)** Wound-healing capacities of *FGFR4-Gly*- and *GFP*-transduced control sublines of U251-MG *(left panel)* and BTL1529 *(right panel)* are depicted. One representative experiment per cell line is shown. Two-way ANOVA: **p<0.01,*** p<0.001

Figure S7

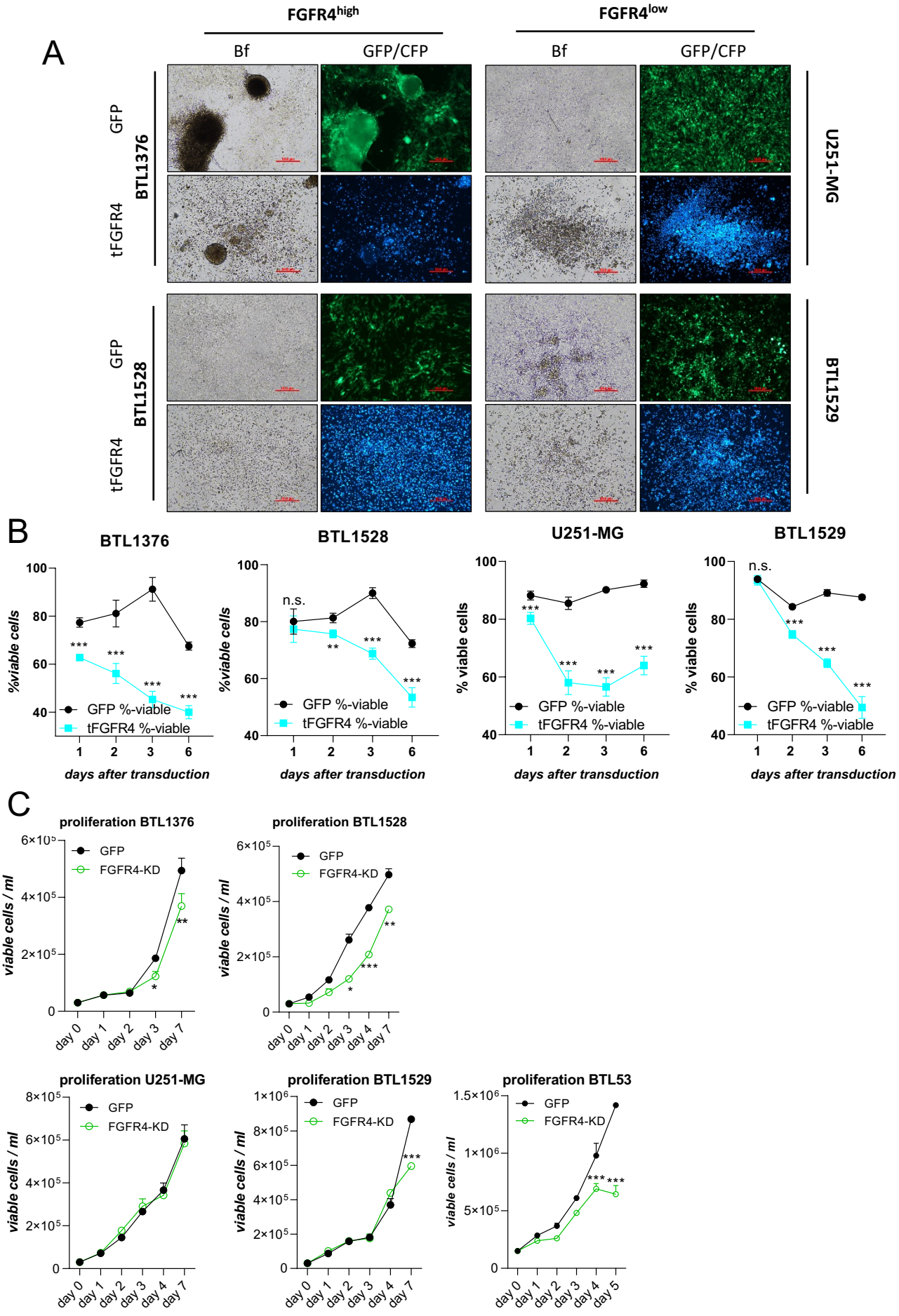
A
FGFR4high
FGFR4low
Bf
GFP/CFP
GFP
tFGFR4
BTL1376
BTL1528
U251-MG
BTL1529
B
BTL1376
BTL1528
U251-MG
BTL1529
%viable cells
% viable cells
GFP %-viable
tFGFR4 %-viable
n.s.
days after transduction
C
proliferation BTL1376
proliferation BTL1528
proliferation U251-MG
proliferation BTL1529
proliferation BTL53
viable cells / ml
GFP
FGFR4-KD

Supplementary Figure S7. Anti-proliferative effects of FGFR4 inactivation in GBM cells. Viability/proliferation assays of the indicated cell models upon *tFGFR4* **(A+B)**, *FGFR4-KD (K504M)* **(C)** or *GFP* transduction were performed for the indicated time frame. **(A)** Representative photomicrographs after 6 days of *tFGFR4* (CFP) or *GFP* transduction are depicted. Scale bars indicate 1000µm. Bf = bright field. **(B+C)** The percentage of viable cells, measured by CASY cell counter, are depicted at the indicated time points. Results are given as mean +/- SD from one representative out of three independent experiments performed in duplicates. **(C)** Significance levels in **(B+C)** were quantified using 2-way ANOVA with Bonferroni correction. * $p<0.05$, ** $p<0.01$, *** $p<0.001$, n.s. = not significant

Figure S8

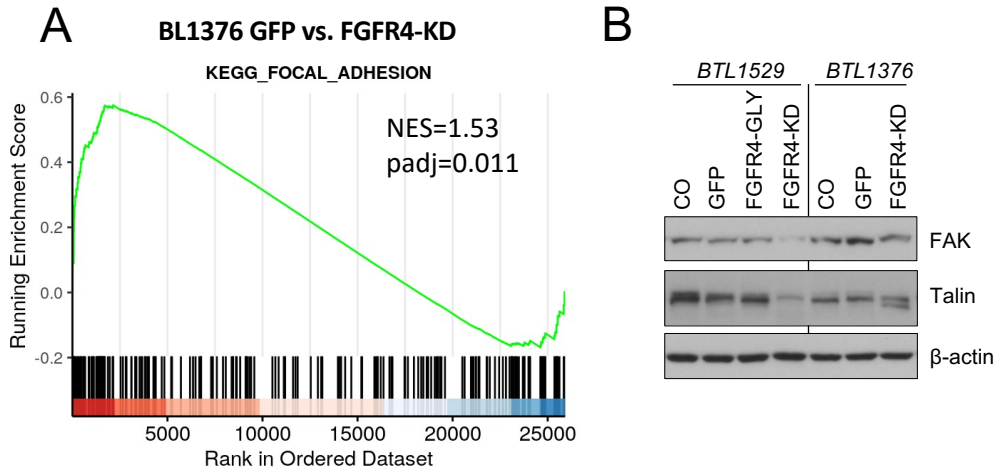
A
BL1376 GFP vs. FGFR4-KD
KEGG_FOCAL_ADHESION
NES=1.53
padj=0.011
Running Enrichment Score
Rank in Ordered Dataset
B
BTL1529
BTL1376
CO
GFP
FGFR4-GLY
FGFR4-KD
FAK
Talin
β-actin

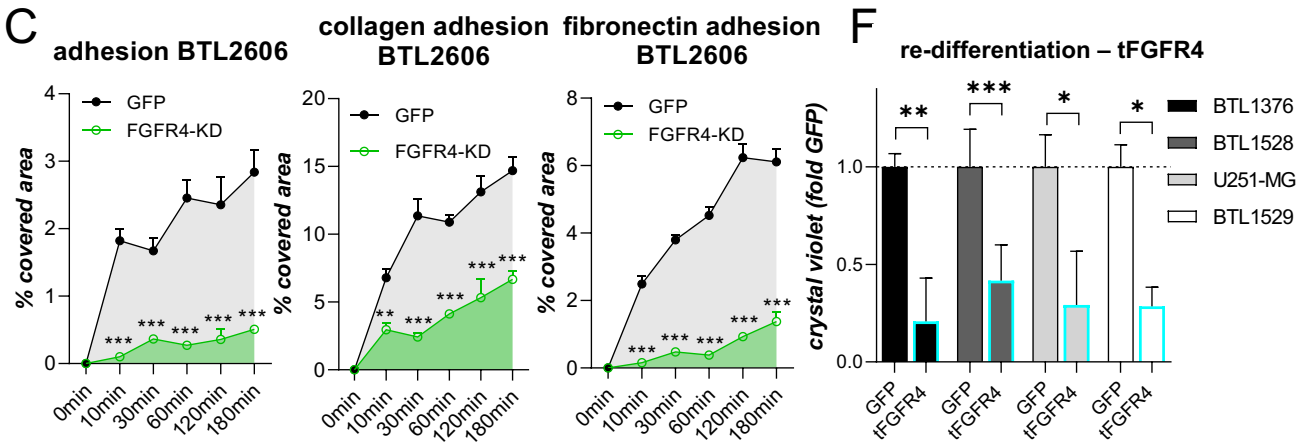
C
adhesion BTL2606
collagen adhesion BTL2606
fibronectin adhesion BTL2606
GFP
FGFR4-KD
% covered area
0min
10min
30min
60min
120min
180min
F
re-differentiation – tFGFR4
crystal violet (fold GFP)
BTL1376
BTL1528
U251-MG
BTL1529
GFP
tFGFR4

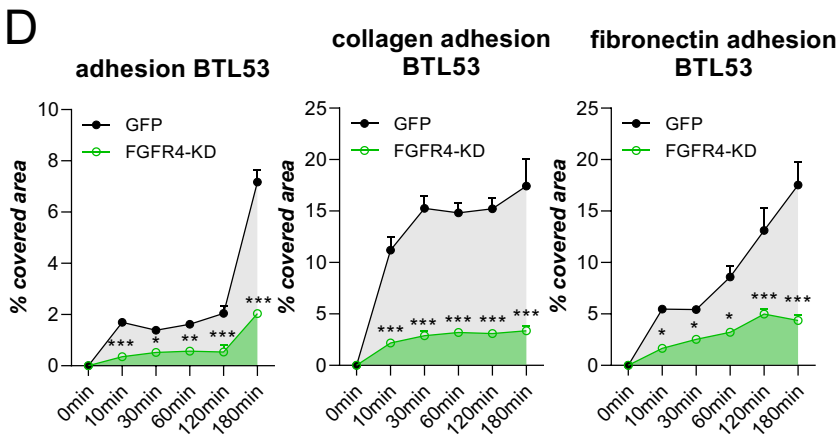
D
adhesion BTL53
collagen adhesion BTL53
fibronectin adhesion BTL53
GFP
FGFR4-KD
% covered area
0min
10min
30min
60min
120min
180min

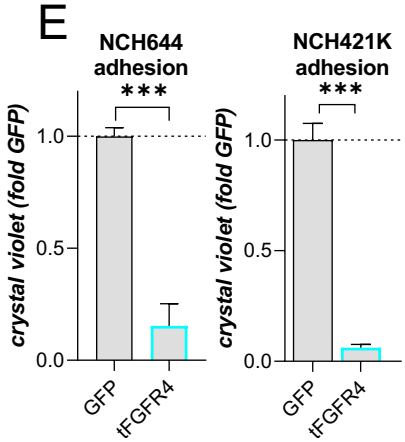
E
NCH644 adhesion
NCH421K adhesion
crystal violet (fold GFP)
GFP
tFGFR4

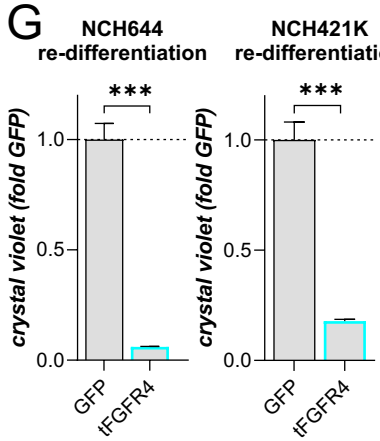
G
NCH644 re-differentiation
NCH421K re-differentiation
crystal violet (fold GFP)
GFP
tFGFR4

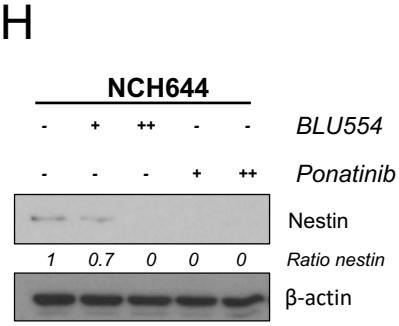
H
NCH644
BLU554
Ponatinib
Nestin
Ratio nestin
1
0.7
0
0
0
β-actin

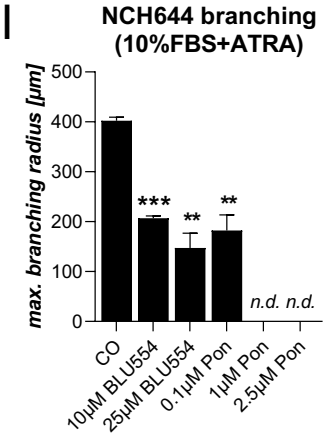
I
NCH644 branching (10%FBS+ATRA)
max. branching radius [µm]
n.d. n.d.
CO
10µM BLU554
25µM BLU554
0.1µM Pon
1µM Pon
2.5µM Pon

Supplementary Figure S8. FGFR4 blockade impairs focal adhesion capacity of glioma cells and GSCs. (A) GSEA revealed altered expression profiles of genes associated to the *KEGG Focal Adhesion* pathway of BTL1376 *GFP* versus *FGFR4-KD (K504M)* sublines. NES = normalized enrichment score, padj = adjusted p-value. **(B)** FAK and talin protein expression levels of *FGFR4-Gly-, FGFR4-KD(K504M)- and GFP*-transduced GBM models, as well as untransduced controls (Co) were detected by Western blot analyses. β-actin served as loading control. **(C-E)** Adhesion capacity towards cell culture polystyrene of the endogenously *FGFR4^{low}* BTL2606 and BTL53 GBM models **(C+D** left panels**)** and NCH644 and NCH421K GSC models **(E)** was analyzed upon *tFGFR4* or *GFP* transduction. Additionally, adhesion capacity of GBM models towards collagen **(C+D** middle panels**)** or fibronectin **(C+D** right panels**)** was analyzed. **(F+G)** Re-differentiation capacities of the indicated GBM **(F)** and GSC **(G)** spheroids upon FGFR4 inactivation using the *tFGFR4* adenovirus were evaluated and compared to *GFP*-transduced controls (set to 1). Cells were transduced with the respective adenovirus (100moi) and kept under serum-deprived conditions. After 5 days, spheres were re-plated in serum-supplemented growth medium. Re-differentiation capacity of the GBM spheroids after another 5 days was analyzed using crystal violet staining. Results are given as mean +/- SEM from three independent experiments. **(H)** Nestin expression was analyzed in NCH644 cells treated with 10µM (+) or 25µM (++) BLU554, or 1µM (+) / 2.5µM (++) ponatinib for 20h by Western blots. β-actin served as loading control. Ratios indicate expression normalized to β-actin. **(I)** Differentiation capacity of the GSC model NCH644 was analyzed upon stimulation with serum-supplemented medium and all-trans retinoic acid (ATRA). Cells were seeded as single cells in GSC medium and treated with the FGFR4-targeting inhibitors BLU554 or ponatinib (Pon) as indicated. After 72h, spheroids were re-seeded in serum-supplemented medium with ATRA and re-treated as indicated. Microphotographs were taken after 72h and results are given as maximal radius from sphere center (µm, mean +/- SD) from two independent experiments performed in duplicates. Significance levels were quantified using 2-way ANOVA with Bonferroni correction **(C,D,F,I)** or Student's t-tests **(E,G)**: * $p<0.05$, ** $p<0.01$, *** $p<0.001$, n.d. not detected.

Figure S9

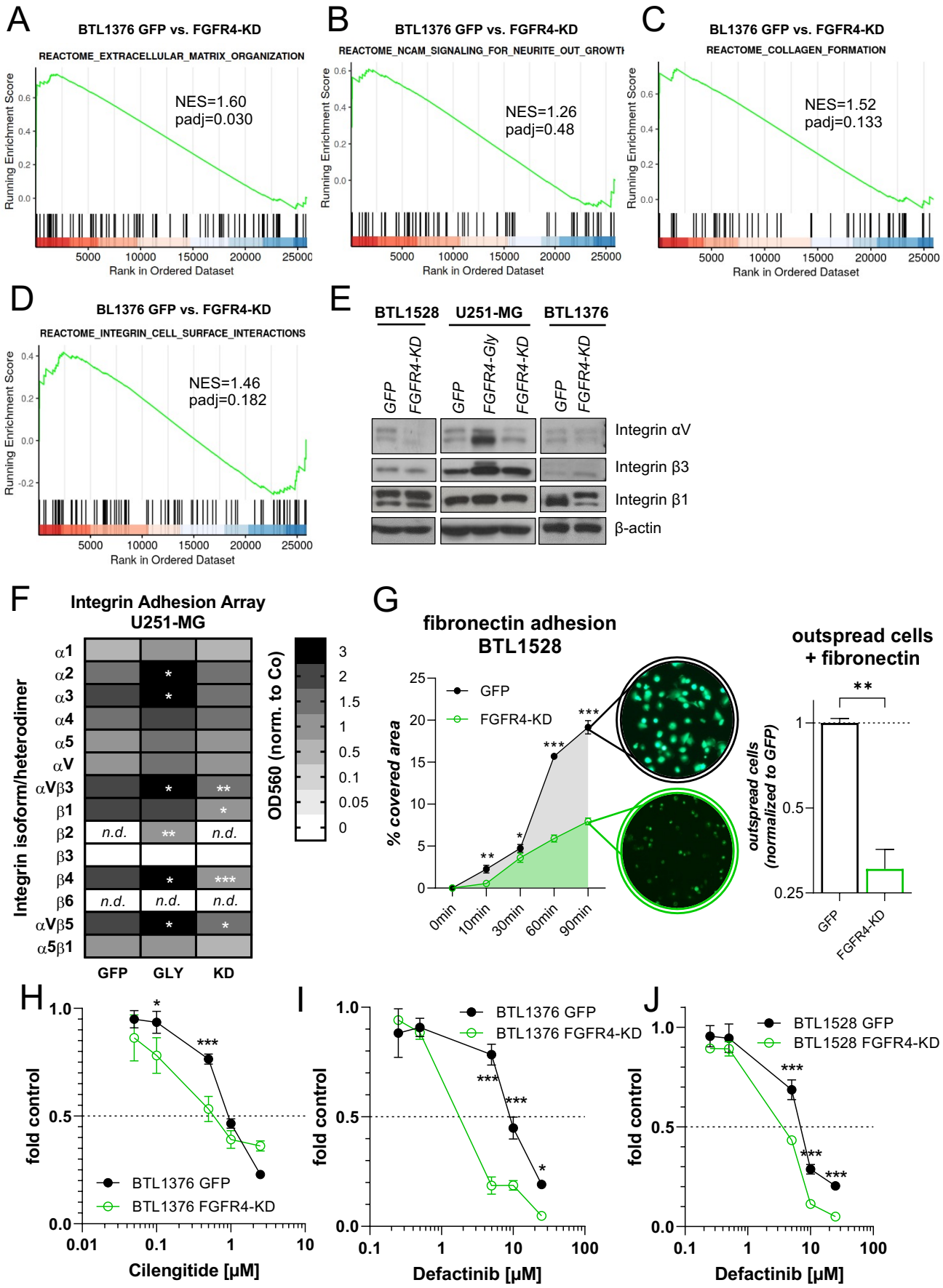
A
BTL1376 GFP vs. FGFR4-KD
REACTOME_EXTRACELLULAR_MATRIX_ORGANIZATION
NES=1.60
padj=0.030
B
BTL1376 GFP vs. FGFR4-KD
REACTOME_NCAM_SIGNALING_FOR_NEURITE_OUT_GROWTH
NES=1.26
padj=0.48
C
BL1376 GFP vs. FGFR4-KD
REACTOME_COLLAGEN_FORMATION
NES=1.52
padj=0.133
Running Enrichment Score
Rank in Ordered Dataset
D
BL1376 GFP vs. FGFR4-KD
REACTOME_INTEGRIN_CELL_SURFACE_INTERACTIONS
NES=1.46
padj=0.182
E
BTL1528
U251-MG
BTL1376
GFP
FGFR4-KD
FGFR4-Gly
Integrin αV
Integrin β3
Integrin β1
β-actin
F
Integrin Adhesion Array
U251-MG
Integrin isoform/heterodimer
α1
α2
α3
α4
α5
αV
αVβ3
β1
β2
β3
β4
β6
αVβ5
α5β1
n.d.
GFP
GLY
KD
OD560 (norm. to Co)
G
fibronectin adhesion
BTL1528
% covered area
0min
10min
30min
60min
90min
outspread cells
+ fibronectin
outspread cells
(normalized to GFP)
H
fold control
Cilengitide [μM]
BTL1376 GFP
BTL1376 FGFR4-KD
I
Defactinib [μM]
J
BTL1528 GFP
BTL1528 FGFR4-KD

Supplementary Figure S9. FGFR4 inactivation drives loss of integrin and collagen networks in GBM resulting in decreased fibronectin adhesion. (A-D) GSEA of BTL1376 *GFP* versus *FGFR4-KD (K504M)* gene expression data revealed altered expression of genes involved in the depicted *REACTOME* pathways. NES = normalized enrichment score, padj = adjusted p-value. **(E)** Integrin αV, β3 and β1 protein expression levels of the indicated cell models and sublines were analyzed by Western blotting. β-actin served as loading control. **(F)** Integrin-mediated cell adhesion arrays of the endogenously *FGFR4^{low}* GBM model U251-MG as compared to the respective FGFR4-GLY- (GLY) and FGFR4-KD-transduced (KD) subclones are shown. Cell adhesion was analyzed by absorbance measurement following cell staining in duplicates. Statistical significance was tested by 2-way ANOVA with Bonferroni correction. **(G)** Adhesion capacity towards fibronectin was analyzed in BTL1528 *FGFR4-KD (K504M)*- and *GFP*-transduced cells. Plates were coated with fibronectin and cells were incubated for the indicated time points. The percentage of the area coated by cells is given as mean +/- SD from one representative out of three independent experiments *(left panel)*. Significance levels were quantified using 2-way ANOVA with Bonferroni correction. Photomicrographs of time point 90min are shown exemplarily. The number of outspread, fully attached cells was counted and data are given relative to the *GFP*-transduced controls for time point 90min *(right panel).* Student's t-test was performed. **(H-J)** Impact of treatment with cilengitide **(H)** or defactinib **(I+J)** as indicated on the viability of BTL1376 **(H+I)** and BTL1528 **(J)** *FGFR4-KD(K504M)*- and *GFP*-transduced GBM sublines is shown. One representative out of three independent experiments in triplicates is depicted (mean of triplicates ± SD). 2-way ANOVA with Bonferroni correction was performed. In all cases: n.d. = not detected, * $p<0.05$, ** $p<0.01$, *** $p<0.001$.

Figure S10

A

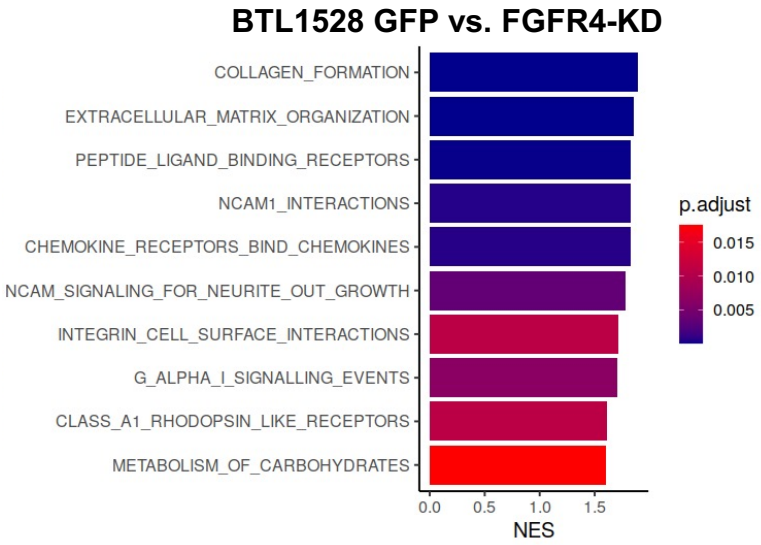

B

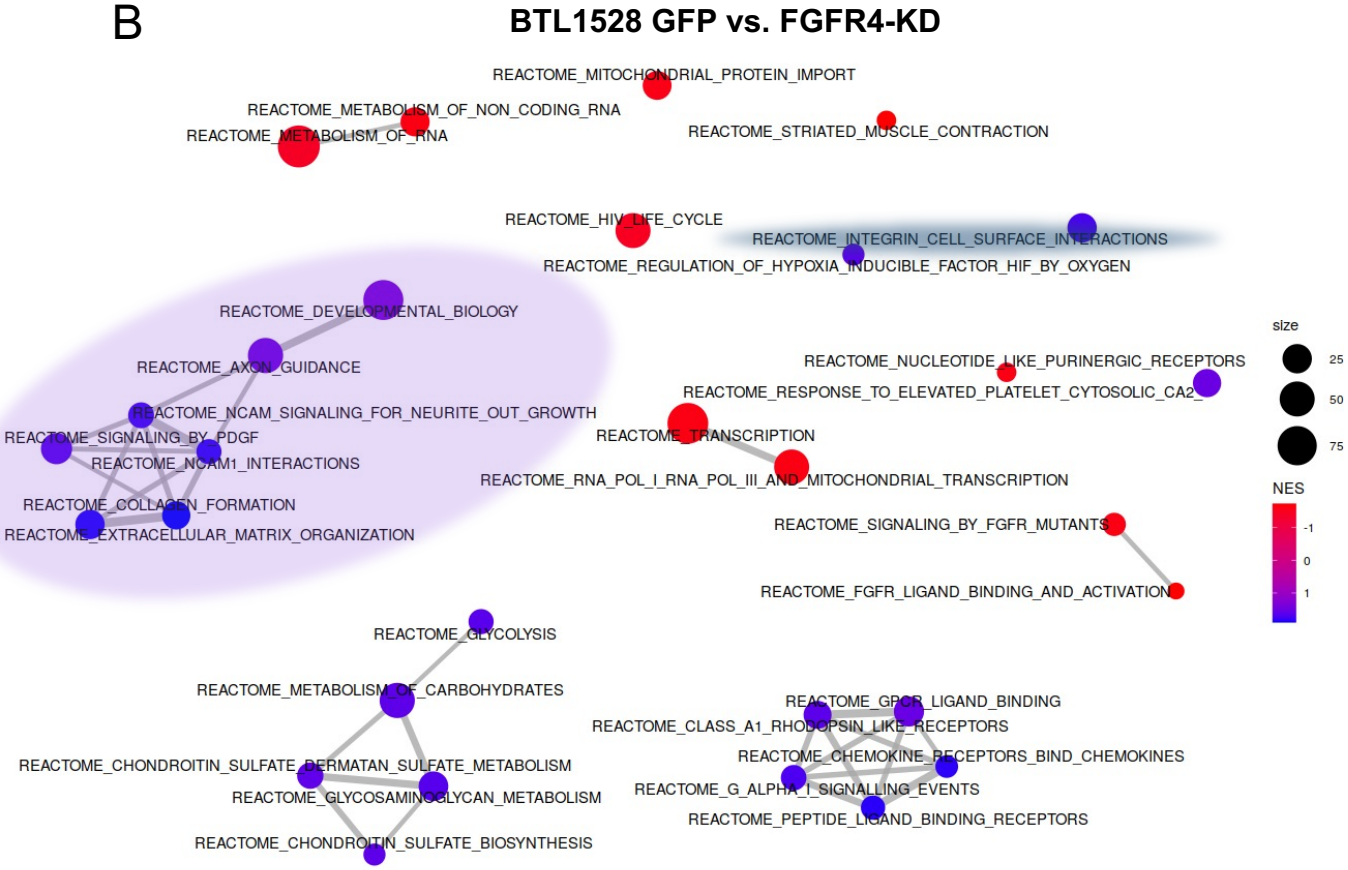

Supplementary Figure S10. Gene ontologies related to FGFR4 blockade cluster in functional modules. (A) The top 10 (ranked by NES) *REACTOME* ontologies in BTL1528 *GFP*- versus *FGFR4-KD(K504M)*-transduced subclones are depicted as bar plot. **(B)** Enrichment map of the top 30 (ranked by NES, p-adjust<0.05) *REACTOME* gene ontologies in BTL1528 *GFP*- versus *FGFR4-KD(K504M)*-expressing GBM sublines is illustrated. Edge size indicates the grade of overlap in the respective gene sets. Node size indicates number of altered genes per gene set. NES=normalized enrichment score.